# $\mathcal{PT}$-symmetric oligomers: Analytical solutions, linear stability, and nonlinear dynamics

K. Li and P. G. Kevrekidis

*Department of Mathematics and Statistics, University of Massachusetts, Amherst, Massachusetts 01003-4515, USA*
(Received 10 February 2011; revised manuscript received 15 April 2011; published 30 June 2011)

In the present work we focus on the case of (few-site) configurations respecting the parity-time ($\mathcal{PT}$) symmetry, i.e., with a spatially odd gain-loss profile. We examine the case of such "oligomers" with not only two sites, as in earlier works, but also the cases of three and four sites. While in the former case of recent experimental interest the picture of existing stationary solutions and their stability is fairly straightforward, the latter cases reveal a considerable additional complexity of solutions, including ones that exist past the linear $\mathcal{PT}$-symmetry breaking point in the case of the trimer, and symmetry-breaking bifurcations, as well as more complex, even asymmetric solutions in the case of the quadrimer with nontrivial properties in their linear stability and in their nonlinear dynamics. The linearization around the obtained solutions and their dynamical evolution, when unstable, are discussed.

## I. INTRODUCTION

Over the past decade, the examination of Hamiltonian nonlinear dynamical lattices, as well as that of continuum systems with periodic potentials, has been a subject of intense investigation [1]. The motivation for such studies stems from a variety of physical settings including, among others, the themes of optical beam dynamics in coupled waveguide arrays or optically induced photonic lattices in photorefractive crystals [2], the temporal evolution of Bose-Einstein condensates (BECs) in optical lattices [3], and the DNA double-strand denaturation in biophysics [4]. One of the common focal points among all of these areas has been the intense study of the existence, stability, and dynamical properties of their nonlinear (often localized in the form of solitary waves) solutions, which are of principal interest and experimental observability within various applications; see [5] for a relevant recent review.

On the other hand, as the understanding of the conservative aspects of such systems comes to a point of maturation, a number of interesting variants thereof arise. A canonical one concerns the examination of the effects of damping and driving that not only yield novel theoretical solutions (see, as an example, [6]), but also are inherently relevant to applications (again, see, for a recent example, [7]). A more exotic variant, however, which in the past couple of years has gained considerable momentum, especially due to the recent experiments of [8], is that of parity-time ($\mathcal{PT}$)-symmetric dynamical lattices. This theme follows the pioneering realization of Bender and coworkers [9] that non-Hermitian Hamiltonians can still yield real spectra, provided that they respect the parity ($\mathcal{P}$) and time-reversal ($\mathcal{T}$) symmetries. Practically, in the presence of a (generally complex) potential, the relevant transformations imply that the potential satisfies the condition $V(x) = V^\star(-x)$. In nonlinear optics, the interest in such applications was initiated by the key contributions of Christodoulides and co-workers [10], which considered solitary waves as well as linear (Floquet-Bloch) eigenmodes in linear periodic potentials satisfying the above condition, and also included the effects of Kerr nonlinearity and observed how the properties of such waves were modified by the genuinely complex, yet $\mathcal{PT}$-symmetric potentials. Such considerations have also been extended to the case of $\mathcal{PT}$-symmetric nonlinear lattices in [11].

Recently, motivated by the experimental possibilities and the relevant realization of a $\mathcal{PT}$ "coupler" in [8], there has been an interest in merging the experience of the above two areas, leading to the consideration of $\mathcal{PT}$-symmetric settings but for genuinely discrete media. In that vein, the experimentally probed two-site system has been considered in the work of [12], where it was shown that it can operate as a unidirectional optical valve, as well as in the study of [13] regarding the role of nonlinearity in allowing (if sufficiently weak) or suppressing (if sufficiently strong) time reversals of the exchanges of optical power between the sites. Another recent example consisted of the generalization of [14] where a lattice of coupled gain-loss dimers was considered. This theme has also been considered in the BEC literature and in the context of the so-called leaky Bose-Hubbard dimers (allowing, e.g., the tunneling escape of atoms from one of the wells of a double-well potential). There, a variant of the model considered below has been self-consistently derived in the mean-field approximation [15] and the correspondence of its classical with the full quantum behavior has been explored [16].

Our aim in the present work is to revisit the examination of the $\mathcal{PT}$-symmetric coupler and to give a simple and complete characterization of the existence and stability properties of its stationary solutions. It should be noted that this aspect has been partly addressed in both [12] and [13]. Nevertheless, we aim to give a characterization thereof as a preamble toward the more complex (and thus, arguably, more interesting) generalization to what we call "$\mathcal{PT}$-symmetric oligomers," namely, the consideration of a $\mathcal{PT}$-symmetric trimer and a $\mathcal{PT}$-symmetric quadrimer. Our aim here is to explore how the complexity of the problem expands as more sites are added in order to offer a glimpse of how such oligomers gradually give way to the elaborate phenomenology of a $\mathcal{PT}$-symmetric lattice. We illustrate, for example, how it is possible in the case of a trimer to identify stationary solutions which exist past the limit of linear $\mathcal{PT}$-symmetry breaking (something which is not possible in the dimer case). We then proceed to illustrate how the phenomenology of the quadrimer is even richer and more complex, featuring, among others, asymmetric solutions with a reduced symmetry spectrum different from the case of both the dimer and the trimer.

Our presentation will be structured as follows. In Sec. II, we consider the fundamental (and previously considered) dimer case. We use this as a benchmark for the presentation of our methods and results. We then turn to the more complex trimer case in Sec. III (and the periodic variant thereof in Sec. IV) and conclude with our results on the quadrimer in Sec. V. Finally, Sec. VI summarizes our findings and presents some interesting questions for further study.

## II. DIMER

We start our considerations from the so-called $\mathcal{PT}$-symmetric coupler or dimer (as we will call it hereafter). In this case, the dynamical equations are of the form

$$
\begin{aligned}
i\dot{u}_1 &= -ku_2 - |u_1|^2 u_1 - i\gamma u_1, \\
i\dot{u}_2 &= -ku_1 - |u_2|^2 u_2 + i\gamma u_2.
\end{aligned}
\tag{1}
$$

The model of Eq. (1) considers the linear $\mathcal{PT}$-symmetric dimer experimentally examined in [8], as augmented by the Kerr nonlinearity relevant, e.g., to optical waveguides; see also [12,13]. The overdot denotes the derivative with respect to the evolution variable, which in optical applications is the propagation distance. In what follows, we will denote this variable by $t$ (to indicate its evolutionary nature). We seek stationary solutions of the form $u_1 = \exp(iEt)a$ and $u_2 = \exp(iEt)b$. Then the stationary equations arise:

$$
\begin{aligned}
Ea &= kb + |a|^2 a + i\gamma a, \\
Eb &= ka + |b|^2 b - i\gamma b.
\end{aligned}
\tag{2}
$$

Using a generic polar representation of the two "sites" $a = Ae^{i\phi_a}$ and $b = Be^{i\phi_b}$, we are led to the following algebraic conditions for the two existing branches of solutions (notice the $\pm$ sign distinguishing between them):

$$
A^2 = B^2 = E \pm \sqrt{k^2 - \gamma^2},
\tag{3}
$$

$$
\sin(\phi_b - \phi_a) = -\frac{\gamma}{k}.
\tag{4}
$$

The fundamental difference of such solutions from their standard Hamiltonian ($\gamma = 0$) counterpart is that the latter were lacking the "flux condition" of Eq. (4). This dictated a selection of the phases so that no phase current would arise between the sites. On the contrary, in $\mathcal{PT}$-symmetric settings, the phase flux is nontrivial and must, in fact, be consonant with the gain-loss pattern of the coupler.

Figure 1 shows the profile of the two branches. The first branch $u^{(1)}$ corresponding to the $(-)$ sign in Eq. (3) is stable when $\gamma^2 \leqslant k^2 - E^2/4$, whereas the second branch $u^{(2)}$ is always stable. The linearization around these branches can be performed explicitly, yielding the nonzero eigenvalue pairs $\pm 2i\sqrt{2(k^2-\gamma^2)-E\sqrt{k^2-\gamma^2}}$ for the first and $\pm 2i\sqrt{2(k^2-\gamma^2)+E\sqrt{k^2-\gamma^2}}$ for the second (notice that the latter can never become real).

It is relevant to note here that the two branches "die" in a saddle-center bifurcation at $\gamma = k$, as shown in the figure. Importantly, this coincides with the linear limit $\gamma_{\mathcal{PT}} = k$ of the $\mathcal{PT}$ symmetry breaking, since the eigenvalues of the linear problem are $\lambda = \pm\sqrt{k^2 - \gamma^2}$. Hence, the nonlinear solutions terminate where the linear problem eigenfunctions yield an imaginary pair, predisposing us for an asymmetric evolution
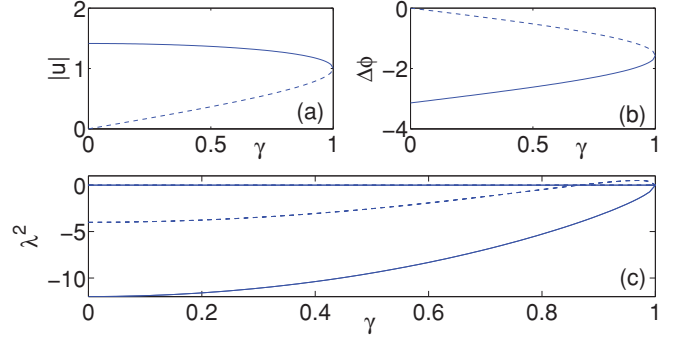


FIG. 1. (Color online) The two branches of solutions for the dimer problem are shown for parameter values $k = E = 1$. (a) The amplitude of the sites, (b) their relative phase, and (c) the (nontrivial) squared eigenvalue of the two branches. The solid line corresponds to the always stable branch $u^{(2)}$, while the dashed line corresponds to the branch $u^{(1)}$, which acquires a real eigenvalue pair above a certain $\gamma = \sqrt{k^2 - E^2/4}$.

past this critical point (for all initial data). The dynamical evolution of the dimer is shown first for a case of $\gamma < k$ (in which $u^{(1)}$ is unstable, while $u^{(2)}$ is stable) in Fig. 2. The evolution of the instability of $u^{(1)}$ leads to an asymmetric distribution of the power in the coupler, despite the fact that parametrically we are below the linear critical point (for the $\mathcal{PT}$-symmetry breaking). Notice that in all the cases, also below, where a stationary solution exists for the parameter values for which it is initialized, dynamical instabilities arise only through the amplification of roundoff errors, i.e., a numerically exact solution up to $10^{-8}$ is typically used as an initial condition in the system. Naturally, beyond $\gamma = k$, as shown in Fig. 3, all initial data yield such an asymmetric evolution.

## III. TRIMER

We now turn to the case of the trimer where the dynamical equations are

$$
\begin{aligned}
i\dot{u}_1 &= -ku_2 - |u_1|^2 u_1 - i\gamma u_1, \\
i\dot{u}_2 &= -k(u_1 + u_3) - |u_2|^2 u_2, \\
i\dot{u}_3 &= -ku_2 - |u_3|^2 u_3 + i\gamma u_3.
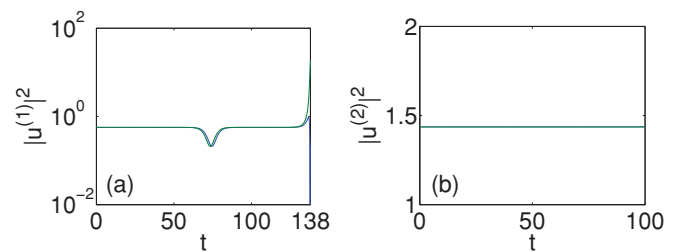\end{aligned}
\tag{5}
$$



FIG. 2. (Color online) Dynamical evolution of initial data belonging to the two branches of stationary solutions of a dimer in the case of $\gamma = 0.9$, $E = k = 1$, which is past the critical point for the instability of the (a) first branch, while the (b) second branch is still dynamically stable. Notice that (a) is plotted in semilog.
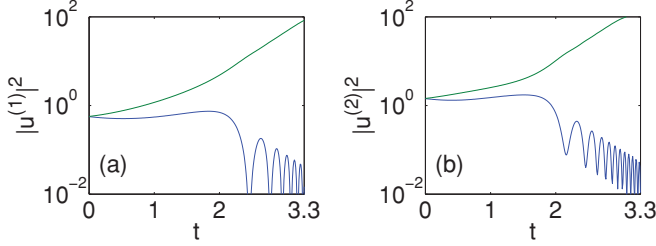
FIG. 3. (Color online) Similar initialization as Fig. 2 of the dimer based on the two branches of stationary solutions (for $\gamma = 0.9$), but now for the case of $\gamma = 1.1$ ($E = k = 1$). The asymmetric evolution of the coupler past the linear $\mathcal{PT}$-symmetric threshold can be clearly discerned. Both are plotted in semilog.

Seeking, once again, stationary solutions leads to the algebraic equations

$$Ea = kb + |a|^2 a + i\gamma a,$$
$$Eb = k(a + c) + |b|^2 b,$$
$$Ec = kb + |c|^2 c - i\gamma c. \qquad (6)$$

In this case too, it is helpful to use the polar representation for the three sites in the form $a = Ae^{i\phi_a}, b = Be^{i\phi_b}, c = Ce^{i\phi_c}$, which, in turn, leads to the algebraic equations of the form

$$A = C, \qquad (7)$$
$$B^4 - EB^2 + 2EA^2 - 2A^4 = 0, \qquad (8)$$
$$\sin(\phi_b - \phi_a) = -\sin(\phi_b - \phi_c) = -\frac{\gamma A}{kB}, \qquad (9)$$
$$\cos(\phi_a - \phi_b) = \cos(\phi_b - \phi_c) = \frac{EA - A^3}{kB}. \qquad (10)$$

Notice how the presence of the gain-loss spatial profile along the three sites induces a spatial phase distribution and enforces the condition of a symmetric amplitude profile with the first and third site sharing the same amplitude. This phase distribution would be trivial (relative phases of 0 or $\pi$) in the $\gamma = 0$ case.

A typical example of the branches that may arise in the case of the trimer is shown in Fig. 4 for $E = k = 1$. In this case, we find three distinct branches in the considered interval of parameter values. There are two branches which exist up to the critical point $\gamma = 1.043$. In this interval, one of the two branches, $u^{(1)}$, is mostly unstable (denoted by a dash-dotted line) except for a small interval of $\gamma \in [1, 1.035]$. The other one, $u^{(2)}$, is mostly stable (denoted by a dashed line) except for $\gamma \in [1.035, 1.043]$. The eigenvalues of $u^{(1)}$ and $u^{(2)}$ in $\gamma \in [1.035, 1.043]$ are very close to each other but not identical. Notice that $u^{(1)}$ is unstable due to a complex eigenvalue quartet whose eigenvalues collide on the imaginary axis for $\gamma = 1$ and split into two imaginary pairs, one of which becomes real for $\gamma > 1.035$. Finally, these two branches collide in a saddle-center bifurcation (for $\gamma = 1.043$) and disappear thereafter.

Interestingly, however, these are not the only branches that arise in the trimer case. In particular, as can be seen
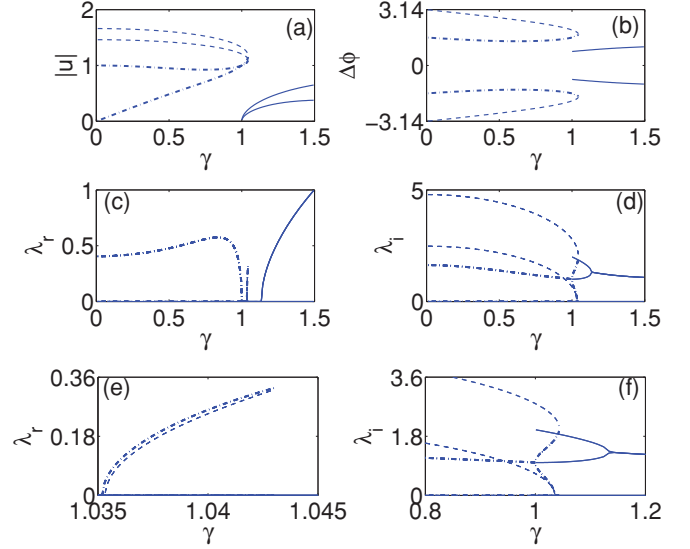


FIG. 4. (Color online) Existence and stability of solutions for the case of the trimer analogous to Fig. 1 with parameters $E = 1$ and $\phi_b$ normalized to 0 (without loss of generality). There are three branches: $u^{(1)}$ (dash-dotted line), $u^{(2)}$ (dashed line), and $u^{(3)}$ (solid line). For each branch, two curves in (a) stand for $A, B, C$ (since $C = A$), and two curves in (b) stand for $\phi_a$ and $\phi_c$. Panels (c) and (d) are the illustration of both real and imaginary parts for the eigenvalues. Panels (e) and (f) are zooms of (c) and (d), respectively.

in Fig. 4, there is a branch of solutions bifurcating from zero (amplitude) for $\gamma > \sqrt{2k^2 - E^2}$, denoted by $u^{(3)}$, which is the solid line in Fig. 4. In our case $E = k = 1$, this branch is only stable for $\gamma < 1.13$, at which point two pairs of imaginary eigenvalues collide and lead to a complex quartet, which renders the branch unstable thereafter. Yet, this branch of solutions has a remarkable trait. In the case of the trimer, the underlying linear problem possesses the following eigenvalues: $0, \pm\sqrt{2k^2 - \gamma^2}$. Hence, the critical point for the existence of real eigenvalues of the linear problem in the case of the $\mathcal{PT}$-symmetric trimer is $\gamma_{\mathcal{PT}} = \sqrt{2}k$ (cf. with the $\gamma_{\mathcal{PT}} = k$ limit of the dimer). Nevertheless, and contrary to the case for the dimer, the third branch of solutions considered above persists beyond this critical point (although it is unstable in that regime).

The evolution of the three distinct branches of solutions, namely, the chiefly unstable one, $u^{(1)}$, the chiefly stable one, $u^{(2)}$, and finally the one persisting past the linearly unstable limit, $u^{(3)}$, is shown, respectively, in Figs. 5, 6, and 7. It can be seen that in accordance with the predictions of our linear stability analysis, the first two branches are stable or unstable in their corresponding regimes, while past the point of existence of these branches ($\gamma = 1.043$), their evolution gives rise to asymmetric dynamics favoring the growth of the power in a single site [or, in some cases, even in two sites; see, e.g., Figs. 5(c) and 6(c)]. On the other hand, for the branch emerging at $\gamma = 1$ and persisting past the linear instability limit, we indeed find it to be stable for $\gamma < 1.13$ and unstable thereafter, again leading to an asymmetric distribution of the power.
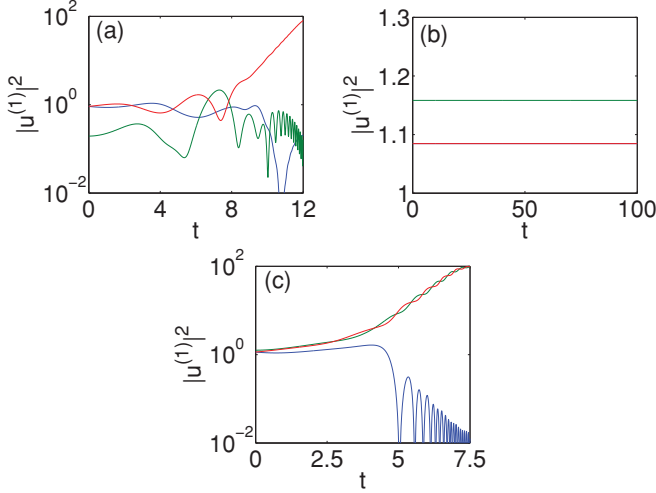
FIG. 5. (Color online) The dynamical evolution of the amplitudes of the three sites of the stationary solution $u^{(1)}$ in the case of $E = k = 1$ for (a) $\gamma = 0.5$, (b) $\gamma = 1.03$, and (c) $\gamma = 1.1$. Panel (c) is initialized with the exact stationary solution for $\gamma = 1.04$ (since for $\gamma = 1.1$, the branch no longer exists as a stationary solution).

## IV. PERIODIC TRIMER

The trimer problem has also been considered in the case of periodic boundary conditions with the dynamical equations being as follows:

$$
\begin{aligned}
i\dot{u}_1 &= -k(u_2 + u_3) - |u_1|^2 u_1 - i\gamma u_1, \\
i\dot{u}_2 &= -k(u_1 + u_3) - |u_2|^2 u_2, \\
i\dot{u}_3 &= -k(u_1 + u_2) - |u_3|^2 u_3 + i\gamma u_3.
\end{aligned}
\tag{11}
$$

It is quite relevant to mention here that the linear version of the problem, in the absence of gain and loss (i.e., for $\gamma = 0$), possesses in this case a pair of degenerate eigenvalues. Notably, as soon as $\gamma \neq 0$, these eigenvalues lead to a complex-conjugate pair. Hence, $\gamma_{\mathcal{PT}} = 0$ in this setting. Nevertheless, we can still mathematically pose (as above) the nonlinear
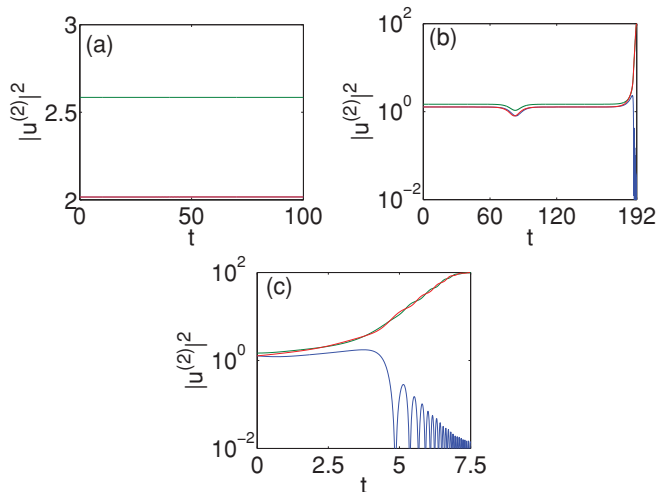


FIG. 6. (Color online) Similar to Fig. 5, but for the case of $u^{(2)}$ and for $E = k = 1$. Panel (c) is again initialized for $\gamma = 1.04$.
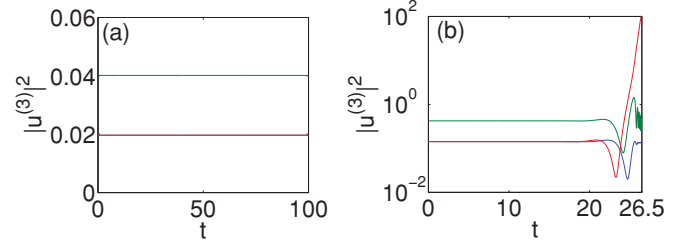


FIG. 7. (Color online) The dynamical evolution for the case of $u^{(3)}$ and for $E = k = 1$; (a) $\gamma = 1.04$ and (b) $\gamma = 1.5$.

problem. Seeking once again stationary solutions thereof leads to the algebraic equations

$$
\begin{aligned}
Ea &= k(b + c) + |a|^2 a + i\gamma a, \\
Eb &= k(a + c) + |b|^2 b, \\
Ec &= k(a + b) + |c|^2 c - i\gamma c.
\end{aligned}
\tag{12}
$$

We also use the polar representation for the three sites in the form $a = Ae^{i\phi_a}, b = Be^{i\phi_b}, c = Ce^{i\phi_c}$. However, in this case, the resulting algebraic equations are too tedious to write down. The numerical results are shown in Fig. 8. Remarkably, the results show that nonlinear branches of solutions (including some which are stable) exist. In fact, there may exist up to four such branches. In the case considered in Fig. 8 with parameters $k = E = 1$, one of the relevant pairs of a stable and unstable trimer state leads to a collision and annihilation through a saddle-center bifurcation for $\gamma = 0.252$. On the other hand, the second pair of branches exists and is stable for $\gamma < 0.66$, but one of the two states becomes unstable thereafter, and a branch-pair terminating saddle-center bifurcation ensues for $\gamma = 0.782$. No solution has been identified for larger gain-loss parameters. Nevertheless, in this case too, it is interesting that stationary (and even stable) nonlinear solutions exist for $\gamma > \gamma_{\mathcal{PT}}$.

## V. QUADRIMER

Finally, we briefly turn to the case of the quadrimer. Here the equations are

$$
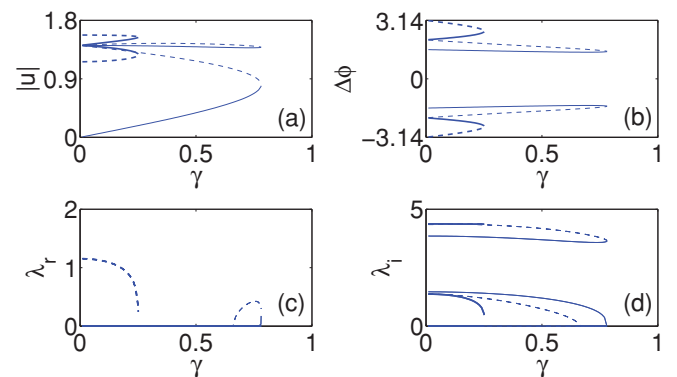i\dot{u}_1 = -ku_2 - |u_1|^2 u_1 - i\gamma u_1,
$$



FIG. 8. Similar to Fig. 4 but with the four branches of the periodic trimer in this case. One pair (thicker lines) disappears at $\gamma = 0.252$. The other pair (thinner lines) ends at $\gamma = 0.782$. One of the solutions of this latter pair already 5 becomes unstable for $\gamma > 0.66$.

$$i\dot{u}_2 = -k(u_1 + u_3) - |u_2|^2 u_2 - i\gamma u_2,$$
$$i\dot{u}_3 = -k(u_2 + u_4) - |u_3|^2 u_3 + i\gamma u_3, \qquad (13)$$
$$i\dot{u}_4 = -ku_3 - |u_4|^2 u_4 + i\gamma u_4.$$

Notice here that we only consider the case where the first two sites have the same loss and the latter two the same gain. This is by no means necessary, and the gain-loss profile can be generalized to involve two parameters (e.g., $\pm\gamma_1$ and $\pm\gamma_2$ distinct between the different corresponding sites, i.e., the first and fourth ones, as well as the second and third ones). We do not consider this latter case here, due to its more complicated algebraic structure that does not permit the direct analytical results given below. More specifically, in our considered special case, the stationary equations read

$$Ea = kb + |a|^2 a + i\gamma a,$$
$$Eb = k(a + c) + |b|^2 b + i\gamma b,$$
$$Ec = k(b + d) + |c|^2 c - i\gamma c, \qquad (14)$$
$$Ed = kc + |d|^2 d - i\gamma d.$$

The polar representation of the form $a = Ae^{i\phi_a}, b = Be^{i\phi_b}, c = Ce^{i\phi_c}, d = De^{i\phi_d}$ now allows the following reduced algebraic equations:

$$A^2 + B^2 = C^2 + D^2 = E, \qquad (15)$$
$$A^2 B^4 + \gamma^2 A^2 - k^2 B^2 = 0, \qquad (16)$$
$$D^2 C^4 + \gamma^2 D^2 - k^2 C^2 = 0, \qquad (17)$$
$$\sin(\phi_b - \phi_a) = -\frac{\gamma A}{kB}, \qquad (18)$$
$$\sin(\phi_c - \phi_b) = -\frac{\gamma E}{kBC} = -1, \qquad (19)$$
$$\sin(\phi_d - \phi_c) = -\frac{\gamma D}{kC}. \qquad (20)$$

Notice that in this case not only do we have the customary phase profile, but in fact one of the phase differences becomes locked to $\pi/2$ due to the presence of the gain-loss pattern.

Upon reducing the algebraic equations, we obtain

$$(E - B^2)B^4 + \gamma^2(E - B^2) - k^2 B^2 = 0, \qquad (21)$$
$$(E - C^2)C^4 + \gamma^2(E - C^2) - k^2 C^2 = 0, \qquad (22)$$
$$\gamma E = kBC. \qquad (23)$$

This leads to the important conclusion that for this gain-loss profile in the case of the quadrimer, in contrast to the cases of the dimer and trimer, one of the parameters $E$, $k$, or $\gamma$ is determined by the other two; i.e., not all three of these parameters can be picked independently in order to give rise to a solution of the quadrimer.

We hereby set $E = 1$, and increase $\gamma$ from 0 as before; then $k$ can be obtained self-consistently from the above equations. Therefore, once $E$ and $\gamma$ are fixed, the solutions of the quadrimer problem are fully determined. We now present three branches of solutions that arise in this setting as we increase $\gamma$. These are shown in the panels of Fig. 9. There are two classes of solutions here. The solid curve $u^{(1)}$ corresponds to a fully asymmetric, always unstable branch with $A$, $B$, $C$, $D$ distinct, i.e., something that is unique (among the settings considered herein) to the quadrimer. On the other hand, the
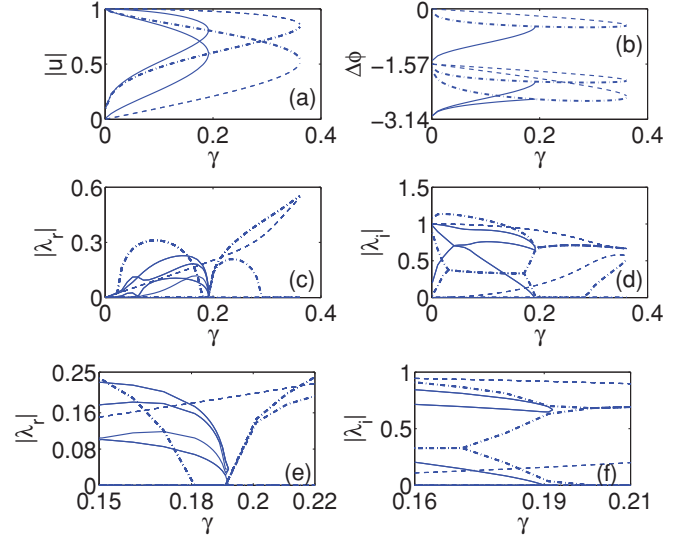


FIG. 9. (Color online) Three branches of solutions for the quadrimer problem with parameters $E = 1$ and $\phi_a$ normalized to 0: the solid lines denote the asymmetric branch $u^{(1)}$, while the dashed and dash-dotted lines denote the symmetric branches $u^{(2)}$ and $u^{(3)}$, respectively. For each branch, four curves in (a) stand for $A, B, C, D$ (only two curves for $u^{(2)}$ and $u^{(3)}$ since $A = D, B = C$ in these cases), and three curves in (b) stand for $\phi_b, \phi_c, \phi_d$. Panel (e) and (f) are zooms of (c) and (d), respectively.

dashed curve of the branch $u^{(2)}$ and the dash-dotted curve of the branch $u^{(3)}$ correspond to symmetric branches with amplitudes $A = D$ and $B = C$. Among the two symmetric branches $u^{(2)}$ and $u^{(3)}$ that collide and disappear together in a saddle-center bifurcation at $\gamma = 0.362$, we can observe that the former has a real and two imaginary pairs of eigenvalues being always unstable, while the latter starts out stable, but the collision of two of its imaginary pairs will render it unstable past the critical point of $\gamma = 0.023$. Interestingly the asymmetric branch $u^{(1)}$ and the symmetric branch $u^{(3)}$ appear to collide in a subcritical pitchfork bifurcation that imparts the instability of the asymmetric branch to the symmetric one for $\gamma > 0.193$.

As an aside, we should also note here that in its linear dynamics, the $\mathcal{PT}$-symmetric quadrimer has an interesting difference from the dimer and trimer. In particular, the four linear eigenvalues of the system are

$$\lambda_{1,2} = \pm\sqrt{-\gamma^2 + \frac{k}{2}(3k - \sqrt{-16\gamma^2 + 5k^2})}, \qquad (24)$$

$$\lambda_{3,4} = \pm\sqrt{-\gamma^2 + \frac{k}{2}(3k + \sqrt{-16\gamma^2 + 5k^2})}. \qquad (25)$$

The fundamental difference of this case from the dimer and regular trimer considered above is that these eigenvalues do not become imaginary by crossing through zero. Instead, they become *genuinely complex* through their collision that occurs for $\gamma_{\mathcal{PT}} = \sqrt{5}k/4$, a critical point which is lower than that of the trimer. This could be an experimentally observable signature of the difference of the near linear dynamics of the quadrimer.

The dynamics of these different branches was also considered in Fig. 10. In this case, it can be clearly observed that all three branches tend toward an asymmetric distribution of
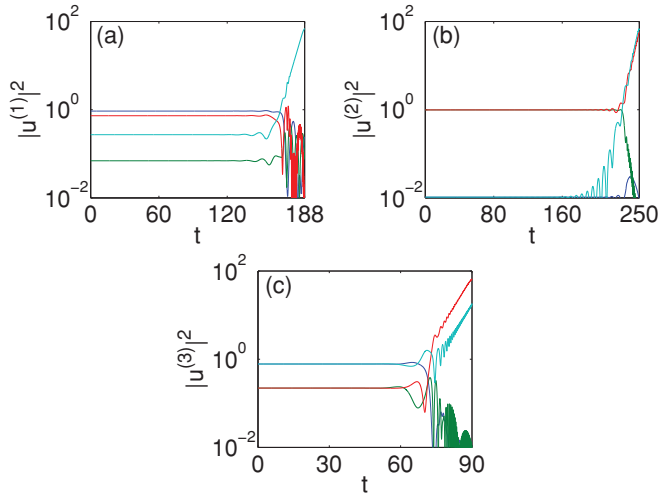
FIG. 10. (Color online) The profile of the dynamical evolution of the three different branches: (a) $u^{(1)}$, (b) $u^{(2)}$, and (c) $u^{(3)}$ of a quadrimer in the case of $E = 1$ and $\gamma = 0.1$.

the power. This favors the two sites (third and fourth) with the gain, although some case examples can be found [see, e.g., Fig. 10(a) for the asymmetric branch] where only one of the two gain sites is favored by the mass evolution.

## VI. CONCLUSIONS

In the present work, we considered the existence, stability, and dynamics of $\mathcal{PT}$-symmetric oligomers, i.e., configurations with few sites. Similar to the recent works of [12,13] and also the experimental investigation of [8], we have started our considerations by a complete characterization of the dimer case, where the two obtained branches of solutions terminate at the critical point of the linear case. However, we illustrated that the trimer and quadrimer feature a number of fundamental differences in comparison with this dimer behavior. In particular, the trimer features branches which exist past the linear critical point (although unstable).
On the other hand, the quadrimer has even richer features: in particular, it possesses completely asymmetric solutions. The bifurcation structure is also richer in the latter problem,

featuring symmetry-breaking pitchfork bifurcations. Another notable feature is that solutions do not exist for arbitrary combinations of coupling, gain-loss parameter, and propagation constant; instead, these parameters appear to be interconnected (at least in the case of a single gain-loss parameter considered herein). Finally, even the linear problem presents interesting variations in this case, featuring the breaking of the real nature of the eigenvalues through two colliding pairs that lead to a quartet occurring for smaller gain-loss parameter values than in the trimer case.

This investigation may be a first step toward obtaining a deeper analytical understanding of the features of $\mathcal{PT}$-symmetric lattices. In such settings, it would be relevant to obtain general conclusions both for the linear dynamics (and how it depends on the gain-loss profile parameters), as well as more importantly for the nonlinear modes, including the solitary waves that may arise. The understanding of such modes and the comparison of their properties to the continuum ones, as well as to the discrete ones in the absence of the gain-loss, would be important directions for future study. From the perspective of oligomers, an additional theme meriting further investigation is the consideration of higher than quadrimer chains and the introduction of elementary topology (i.e., quasi-two-dimensionality) in them. In this case, the topology of the quadrimer may enable additional potential states, including ones that may carry "discrete vorticity" over the plaquette, by analogy to corresponding forms of such states in the standard discrete nonlinear Schrödinger equation (DNLS) setting without gain or loss [1,5]. A detailed understanding of the interplay between topology and the gain-loss symmetry would be of particular value in the context of such states.

[1] S. Aubry, Physica D **103**, 201 (1997); S. Flach and C. R. Willis, Phys. Rep. **295**, 181 (1998); D. Hennig and G. Tsironis, *ibid.* **307**, 333 (1999); P. G. Kevrekidis, K. O. Rasmussen, and A. R. Bishop, Int. J. Mod. Phys. B **15**, 2833 (2001) ; A. Gorbach and S. Flach, Phys. Rep. **467**, 1 (2008).

[2] D. N. Christodoulides, F. Lederer, and Y. Silberberg, Nature (London) **424**, 817 (2003); Yu. S. Kivshar and G. P. Agrawal, *Optical Solitons: From Fibers to Photonic Crystals* (Academic, San Diego, 2003).

[3] P. G. Kevrekidis and D. J. Frantzeskakis, Mod. Phys. Lett. B **18**, 173 (2004); V. V. Konotop and V. A. Brazhnyi, *ibid.* **18**, 627 (2004); O. Morsch and M. Oberthaler, Rev. Mod. Phys. **78**, 179 (2006).

[4] M. Peyrard, Nonlinearity **17**, R1 (2004).

[5] P. G. Kevrekidis, e-print arXiv:1009.3178.

[6] P. Maniadis and S. Flach, Europhys. Lett. **74**, 452 (2006).

[7] J. Cuevas, L. Q. English, P. G. Kevrekidis, and M. Anderson, Phys. Rev. Lett. **102**, 224101 (2009).

[8] C. E. Rüter, K. G. Makris, R. El-Ganainy, D. N. Christodoulides, M. Segev, and D. Kip, Nature Phys. **6**, 192 (2010).

[9] C. M. Bender and S. Boettcher, Phys. Rev. Lett. **80**, 5243 (1998); C. M. Bender, S. Boettcher, and P. N. Meisinger, J. Math. Phys. **40**, 2201 (1999); C. M. Bender, Rep. Prog. Phys. **70**, 947 (2007).

[10] Z. H. Musslimani, K. G. Makris, R. El-Ganainy, and D. N. Christodoulides, Phys. Rev. Lett. **100**, 030402 (2008);

K. G. Makris, R. El-Ganainy, D. N. Christodoulides, and Z. H. Musslimani, Phys. Rev. A **81**, 063807 (2010).

[11] F. Kh. Abdullaev, Y. V. Kartashov, V. V. Konotop, and D. A. Zezyulin, Phys. Rev. A **83**, 041805(R) (2011).

[12] H. Ramezani, T. Kottos, R. El-Ganainy, and D. N. Christodoulides, Phys. Rev. A **82**, 043803 (2010).

[13] A. A. Sukhorukov, Z. Xu, and Yu. S. Kivshar, Phys. Rev. A **82**, 043818 (2010).

[14] M. C. Zheng, D. N. Christodoulides, R. Fleischmann, and T. Kottos, Phys. Rev. A **82**, 010103(R) (2010).

[15] E. M. Graefe, H. J. Korsch, and A. E. Niederle, Phys. Rev. Lett. **101**, 150408 (2008).

[16] E. M. Graefe, H. J. Korsch, and A. E. Niederle, Phys. Rev. A **82**, 013629 (2010).